Ultrasound Micro-Elastography: A New Imaging Modality To Phenotype Hypertension In Rat Models

Roch L. Maurice[a,b], Jérémie Fromageau[a], François Yua[a], Ékatherina Stoyanova[a], Zhao Qin[a], Junzheng Peng[c], Pavel Hamet[d], Johanne Tremblay[c] and Guy Cloutier[a,b]

a Laboratory of Biorheology and Medical Ultrasonics, Research Center, University of Montreal Hospital, Montreal, Quebec
b Department of Radiology, Radio-Oncology and Nuclear Medicine, and Institute of Biomedical Engineering, University of Montreal, Montreal, Quebec
c Laboratory of Cellular Biology of Hypertension, Research Center, University of Montreal Hospital, Montreal, Quebec
d Laboratory of Molecular Medicine, Research Center, University of Montreal Hospital, Montreal, Quebec

ABSTRACT

New ultrasound imaging methods are proposed to non-invasively characterize the mechanical properties of superficial arteries (MicroNIVE) and kidneys (MicroNIKE) in rodents. In MicroNIVE, the vessel wall is compressed/dilated by the blood flow pulsation, whereas time-sequences of high-resolution radio-frequency (RF) ultrasound data are externally acquired. The kinematics of the vascular tissue, assessed with the Lagrangian Speckle Model Estimator (LSME), provides a strain cartography also known as elastogram. Because the LSME assumes linear elasticity conditions, strain is inversely proportional to stiffness, which is an intermediate phenotype of the hypertension (HT) trait. Results are presented for the common carotid artery of spontaneously hypertensive rats (SHR, n = 5) and control normotensive Brown Norway (BN, n = 5) rats. At 15-weeks old, the SHR rats' carotid artery (4.46 ± 1.79 % of strain) was found, on average, stiffer that of the BN's, which exhibited strains of 6.76 ± 1.48 % (p < .059). On the other hand, in MicroNIKE, the kidney is externally compressed with the ultrasound probe while time-sequences of high-resolution RF data are acquired. For the purpose of investigating the feasibility of MicroNIKE, a fresh excised kidney from a Recombinant Inbred (RI) rat was investigated. The elastograms, computed with the LSME, clearly exhibited the medulla with distinct mechanical properties. It is concluded that MicroNIVE and MicroNIKE are promising new imaging tools to non-invasively and longitudinally study the impact of targeted genes on vascular tissue remodeling and nephroangiosclerosis in engineered rat models of HT.

SOMMAIRE

L'hypertension est connue pour entraîner des dommages d'organes incluant les vaisseaux sanguins et les reins. Notamment, des études menées sur des modèles de rongeurs ont permis de démontrer que cette pathologie est influencée par certains facteurs structuraux et fonctionnels touchant les artères, tels l'hypertrophie et le remodelage. En d'autres termes, l'hypertension s'accompagne de modulations des propriétés mécaniques des artères. Similairement, la néphrosclérose est caractérisée par des changements de propriétés mécaniques du tissu rénal. Cet article introduit deux nouvelles modalités d'imagerie ultrasonore ayant pour objectifs la caractérisation non-intrusive des propriétés mécaniques des artères superficielles (MicroNIVE) et des reins (MicroNIKE) de rongeurs. Ceci permettrait d'étudier les artères et les reins affligés par cette pathologie dans leur milieu physiologique naturel. En ce qui concerne la MicroNIVE, la paroi vasculaire est naturellement assujettie à une cinétique induite par le flux sanguin. Un algorithme dédié, connu sous l'appellation de Lagrangian Speckle Model Estimator (LSME), est utilisé pour estimer, à partir de séquences temporelles d'images ultrasonores, le mouvement de la paroi artérielle et en déduire la déformation. Le LSME assumant des conditions d'élasticité linéaire, la déformation est inversement proportionnelle à la rigidité. L'étude, ici reportée, a été effectuée in situ sur des rats hypertendus SHR (n = 5) et normotendus BN (n = 5), âgés de 15 semaines. Il a été observé que la carotide commune des SHR, avec 4.46 ± 1.79 % de déformation, était plus rigide que celle des BN, avec 6.76 ± 1.48 % (p < .059). Une étude préliminaire in vitro, menée sur un rein excisé d'un rat hypertendu, est aussi reportée. Dans ce contexte, une compression externe a été appliquée pour induire une cinétique au tissu rénal lors de l'acquisition des images ultrasonores. La cartographie des déformations obtenue avec le LSME, dite élastogramme, distingue clairement les structures du rein dont la médulla avec une rigidité spécifique. Ces résultats permettent de croire dans le potentiel de la Micro-Élastographie pour des applications ultérieures dans les domaines de la pathophysiologie et de la pharmacogénétique de l'hypertension.

1. INTRODUCTION

Hypertension (HT) afflicts approximately 25% of the world population and only 13% of hypertensive patients have adequate blood pressure (BP) control [1]. HT leads to damage of organs such as the brain, the kidneys, the heart and blood vessels. The lack of controlled blood pressure and the impact on end organs are believed to be the reason that, on a global basis, HT is the leading risk factor for mortality and the third major risk factor for the burden of all diseases in terms of disability adjusted life years [2].

So far, in most studies to detect specific manifestations of HT, *i.e.* to phenotype HT, insights are provided mainly by *ex vivo* experiments using rat models' arteries or organs [3, 4, 5, 6, 7 and 8]. However, since the most important insights on a disease should come from the investigations of the afflicted tissues/organs in the presence of a physiological environment, the development of a non-invasive imaging method for *in situ* investigations of HT in rodents would be of great pathophysiological and pharmaceutical relevance.

Over the past years, researchers have selectively bred rats for high blood pressure to provide animal models of HT; the spontaneously hypertensive rat (SHR) is a very common type of such animal model. On the other hand, animals can also be selected for low blood pressure; that is the case of the Brown Norway (BN) rats, a normotensive strain that is usually considered as a reference in terms of blood pressures. It is worth mentioning that SHR and BN are progenitor strains of the recombinant inbred (RI) rats that are also developed for HT research [9]. Integration of transcriptional profiling and linkage analysis has already been achieved for the RI strain [10, 11]. In this study, carotid artery mechanical properties of SHR and BN rats were investigated to evaluate the potential of a new method, said MicroNIVE, to phenotype HT. This paper also reports preliminary data of MicroNIKE, another new method that aims to mechanically characterize the kidney.

1.1. Hypertension and blood vessel remodeling

It is known that BP is influenced by several structural and functional factors, namely hypertrophy and remodeling of arterial and arteriolar vessels. Regarding the vessel wall, this means that intrinsic alterations of its mechanical properties occur. Indeed, the arterial compliance and distensibility are modulated by HT [12]. Namely, arterial walls become less compliant with HT. Since compliance and distensibility are both dependent on the vascular tissue stiffness, we make the assumption that the vascular tissue elastic modulus, or equivalently the strain when the artery is under stress, constitutes a potential phenotype of HT.

1.2. Hypertension and nephroangiosclerosis

Nephrosclerosis, also known as nephroangiosclerosis, is literally defined as the hardening of kidneys. It is the result of scarring or replacement of the normal renal parenchyma by dense collagenous tissues. High blood pressure is a well-recognized feature in chronic renal disease, but the ability of mild to moderate hypertension to produce renal insufficiency is still poorly understood [7]. Similarly to the blood vessel remodeling context, we make the assumption that the renal tissue stiffness constitutes a potential phenotype of HT.

1.3. Ultrasound elastography

Ophir *et al.* [13] introduced elastography in the early nineties. This imaging modality was defined as biological tissue elasticity or stiffness imaging. Elastography enables the calculation of tissue deformation from sequences of radio-frequency (RF) images acquired at different load levels. Tissue mechanical properties are assessed by analyzing the kinematics of the tissue acoustical signatures within the RF data set. The primary objectives of elastography were to complement B-mode ultrasound imaging as a screening method to detect rigid areas in human breasts [14] and to investigate tissue heterogeneity in prostate cancers [15, 16].

Ultrasound elastography was also proposed for human vessel wall characterization using endovascular catheters [17,18,19,20,21]. Several groups recently proposed different approaches to non-invasively characterize superficial arteries by using standard extra-corporal array transducers [22, 23, 24]. The method was labeled as NIVE, i.e. **N**on-**I**nvasive **V**ascular **E**lastography [24]. Furthermore, in [25], our group reported *in vitro* flow phantom experiments and preliminary *in vivo* results for the carotid arteries of rat models of HT. Being the application of NIVE for the purpose of investigating small vessels in rodents, this method was labeled as MicroNIVE. In MicroNIVE, the vessel wall is naturally compressed/dilated by the blood flow pulsation and no external pulsing of the artery is required to map the strain pattern within the vessel wall. Similarly, the appellation of MicroNIKE was chosen for kidney investigations in small animals.

1.4. Objectives

This paper first reports preliminary data on MicroNIVE. The mechanical properties (namely, strain) of carotid arteries were quantitatively assessed *in situ* in SHR and BN rats. We then addressed the possibility to investigate rodents' kidneys using elastography (MicroNIKE). In this context, *ex vivo* RF data were acquired from a fresh excised RI rat's kidney. In both experimental studies, the Lagrangian speckle model estimator (LSME) [24,25,26] was used to compute strain distributions (or elastograms) within the region of interest (ROI). The sections below give an overview of the animal models, the experimental set-up, and the mathematical model that supports the LSME. Subsequently, results are presented and discussed, with remarks on our final conclusions.

2. MATERIALS

This investigation is conformed with Canadian CCAC ("Canadian Council of Animal Care") guidelines as well as the Guide *for the Care and Use of Laboratory Animals* published by the US National Institutes of Health (NIH Publication No 85-23, revised 1996), and all procedures were approved by the institutional Animal Care Committee of the Centre Hospitalier de l'Université de Montréal (CHUM).

2.1. MicroNIVE animal models

In order to investigate the feasibility of MicroNIVE, time-sequences of ultrasound RF data were acquired on ten 15-week old male rats: 5 normotensive Brown Norway (BN) rats and 5 spontaneously hypertensive rats (SHR), respectively. During ultrasound data acquisition, they were anesthetized by inhalation of 2.5 % isofluorane. The body temperature of each animal was monitored with a rectal probe (Thermalert TH-5, Physitemp Instruments, Clifton, NJ, USA) and maintained at $37 \pm 1^{\circ}C$ by using a heating surface. The systolic blood pressures were measured with a tail-cuff monitoring system (Kent Scientific, model XBP-1000, Torrington, CT, USA). It was measured locally in the tail and consequently it underestimated the systemic pressure. The hairs over the neck were shaved and further removed with a depilatory cream (Nair, Church and Dwight Co., USA). Sequences of RF data were acquired over longitudinal sections of the common carotid artery.

2.2. MicroNIKE animal model

A fresh 1.36 g-weight kidney was harvested from a 94-weeks old male RI rat, just following sacrifice by CO_2 gas inhalation. As illustrated in Fig. 1, for the purpose of acquiring RF data, the kidney was immersed in a gelatin-agar mixture while step-wisely compressed by the ultrasound probe. The probe of the ultrasound scanner was fixed to an extendable arm. The height of the arm was controlled by rotating a screw, which allowed a precise displacement of 1mm by revolution. Five images, corresponding to five steps of compression, were acquired. One step of compression was equivalent to an axial (vertical) displacement of the probe of 0.5 mm.

2.3. Experimental set-up

High-frequency imaging system and acquisition protocol

To allow computing elastograms of the carotid wall and of the excised kidney, a high-resolution ultrasound biomicroscope with access to the RF data (Vevo 660, Visualsonics, Toronto, Canada) was required. The Vevo 660 (Fig. 1c) is equipped with an encapsulated oscillating element transducer. A 40 MHz central frequency probe (f-number = 2, diameter = 3 mm, focal length = 6 mm and bandwidth at –6 dB = 110 %) was

used for the carotid artery scanning, whereas a 20 MHz central frequency probe (f-number = 2, diameter = 3 mm, focal length = 15 mm and bandwidth at –6 dB = 110 %) was used for the kidney. The frame rate was 30 images/s in both cases. The RF signals were digitized with an acquisition board (Gagescope, model 8500 CS, Montreal, QC, Canada) installed in a personal computer. The sampling frequency was 500 MHz in an 8-bit format.

Data pre- and post-processing

The data pre-processing is described in details elsewhere [25]. The elastograms were computed by considering all pairs of consecutive RF images that were digitized, typically 8 RF images per data set. Each elastogram was post-processed using a 1×1 pixel kernel Gaussian-filter to smooth the visual appearance of all images. Regarding the carotid artery elastograms, manual segmentation was performed to display only the strain patterns within the vessel wall.
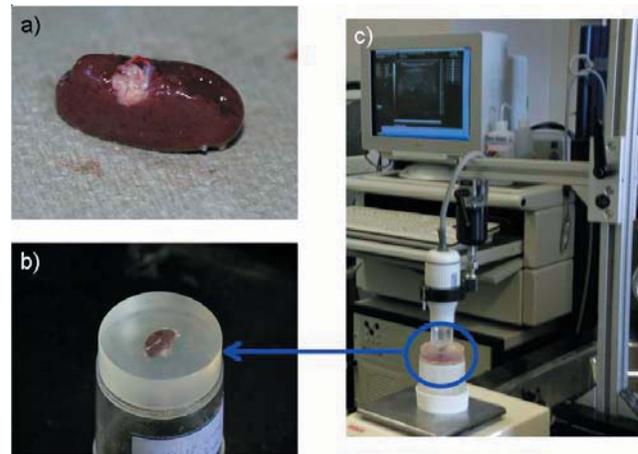

Fig. 1. a) Picture of the RI rat's fresh excised kidney. b) The kidney was immersed in a gelatin-agar mixture. c) Complete picture of the experimental set-up, including the Visualsonics Vevo 660.

3. METHODS

3.1. The Lagrangian speckle model estimator (LSME)

The Lagrangian speckle model estimator (LSME) is a 2D model-based estimator that allows computing the complete 2D-deformation matrix [19], given as:

$$\Delta = \begin{bmatrix} \dfrac{\partial U_x}{\partial x} & \dfrac{\partial U_x}{\partial y} \\ \dfrac{\partial U_r}{\partial x} & \dfrac{\partial U_r}{\partial y} \end{bmatrix}. \tag{1}$$

In this equation, U_y and U_x are the axial and lateral displacement fields, respectively. The four components of Δ, in this specific Cartesian coordinates formulation, are Δ_{yy}, Δ_{yx},

Canadian Acoustics / Acoustique canadienne

Δ_{xx}, and Δ_{xy}, being the axial strain and shear, and the lateral strain and shear, respectively. The map of the distribution of each component of Δ (Δ_{ij}) provides a specific elastogram. It is also worth mentioning that Δ relates the strain tensor ε through the following equation:

$$\varepsilon_{ij}(t) = \frac{1}{2}\left[\Delta_{ij}(t) + \Delta_{ji}(t)\right]. \tag{2}$$

On the other hand, due to the limited lateral resolution of the current ultrasound scanners, axial motion parameters are more accurate. For the purpose of these studies, only the axial strain component ε_{yy} (= Δ_{yy}) was then used to image tissue mechanical properties.

3.2. Implementation of the LSME

To provide distribution of local strains within the region of interest (ROI), the LSME requires subdividing the RF data into several partitions (also known as measurement-windows), for which motion can be assumed as affine [26]. The parameter ε_{yy} was assessed for each partition using the optical flow-based implementation of the LSME [25]. The map of the distribution of ε_{yy} inside each ROI is defined as the elastogram. Each measurement-window was set at 108 µm axially by 312 µm laterally (80 samples × 20 RF lines) with 90 % axial and lateral overlaps. Regarding carotid arteries, comparisons between the BN and SHR were proceeded according to the maximum strain calculated from elastograms computed during the diastolic phase of the cardiac cycle (CC).

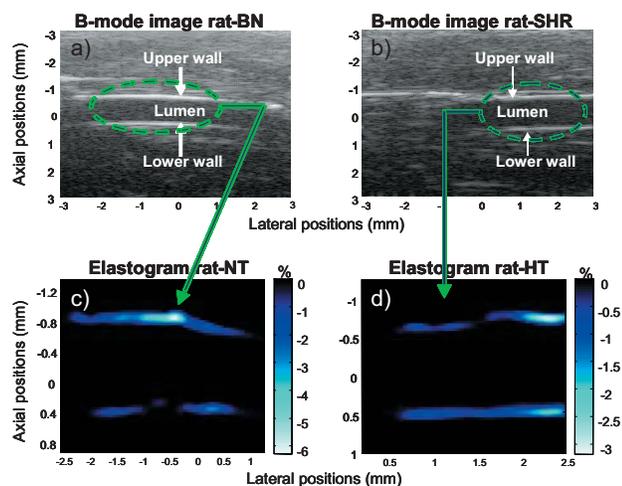## 4. RESULTS

4.1. BN and SHR carotid artery data

Fig. 2. a) and b) display B-mode images of BN and SHR's carotid arteries, respectively. c) and d) are elastograms computed from BN and SHR's carotid RF data, respectively.

The colorbar (in percent) gives the strain and indicates that the SHR's carotid artery is stiffer than that of BN's.

Elastograms were computed for each pair of successive RF images acquired from the SHR's and from the BN's common carotid arteries, typically over one CC. In most cases, it was difficult to have complete longitudinal sections of the artery, consequently only portions of the carotids are displayed on the B-mode images and on the elastograms. Figs 2a and 2b show two B-mode images obtained for one BN and one SHR, respectively. In both cases, the internal diameter of the carotid was around 1 mm, whereas the wall thicknesses were close to 200 µm. Figs 2c and 2d show two elastograms, computed for the BN and the SHR, respectively. The colorbar gives the strain in percent. The negative strain (ε_{yy}) values are indicative of vessel wall dilation (diastolic phase), i.e. lumen area reduction. It is shown that the BN's carotid deforms more than that of the SHR even though the systolic blood pressure (SBP) were higher. In other words, SHRs' arterial walls were, on average, stiffer than that of BN rats.

	SBP (mmHg)	HR (BPM)	S (%)
BN	80 ± 2	316 ± 19	6.76 ± 1.48
SHR	161 ± 12	354 ± 31	4.46 ± 1.79
Values of p	< 0.001	$= 0.052$	$= 0.059$

TABLE 1. Comparisons between SHR and BN. The SBP, HR and strains (S = ε_{yy}) were measured at 15-weeks old. S dictates that the SHR's carotid artery was 1.5 times stiffer than BN's one ($p = 0.059$), whereas the systolic blood pressure (SBP) of the SHR was twice higher than that of the BN ($p < 0.001$).

Table 1 summarizes the comparison between BN (n = 5) and SHR (n = 5) at 15-weeks old (the statistics were obtained with unpaired t-tests). Although the SBP of the SHR was twice that of the BN ($p < 0.001$), the strain (S) of the SHR's carotid artery was, on average, close to 50% less than BN's one ($p = 0.059$), which is indicative of stiffer arteries. The HR of the SHR was, on average, 12% higher than that of BN ($p = 0.052$).
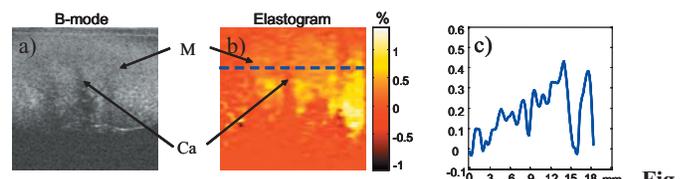
4.2. RI's kidney data

Fig. 3. a) B-mode image of a longitudinal section of the RI's kidney. b) Elastogram of the kidney clearly exhibiting the medulla (denoted M) with specific mechanical properties compared to calyces (denoted Ca). c) Strain plot traced from the elastogram (dotted blue line). The colorbar gives the strain in percent.

Fig. 3a displays a B-mode image acquired from a longitudinal section of the RI's kidney, whereas Fig. 3b shows an elastogram. The kidney medulla is clearly identified with

distinct mechanical properties. Fig. 3c reports a plot of strain values from the elastogram that shows 0.1 % to 0.4 % strain in the medulla. The ascending slope profile of the strain plot is explained in the discussion section.
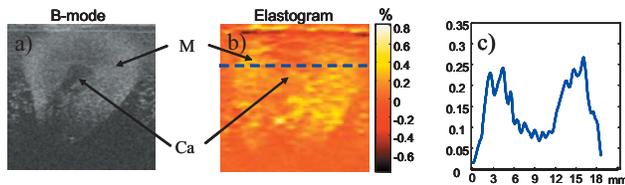

Fig. 4. a) B-mode image of a transverse section of the RI's kidney. b) Elastogram of the kidney clearly exhibiting the presence of the medulla (denoted M) surrounding the calyces (denoted Ca). c) Strain plot traced from the elastogram (dotted blue line). The colorbar gives the strain in percent.

Fig. 4a displays a B-mode image acquired from a transverse section of the RI's kidney, whereas Fig. 4b shows an elastogram. The presence of the medulla surrounding the calyces is clearly observed. Fig. 4c plots strain values from the elastogram. In this case, the medulla is clearly identified with around 0.25 % strain compared to calyces with a lower strain of 0.1%.

5. DISCUSSION

5.1. About the strain estimation

This paper has reported feasibility studies of MicroNIVE and MicroNIKE that propose to phenotype rat models of hypertension using the carotid artery and the kidney mechanical properties, respectively. The proposed ultrasound elastography techniques take advantage of high-resolution radio-frequency (RF) data.

5.2. About MicroNIVE data

An important result of this study was the quantitative observation that normotensive BN's carotid artery at 15-weeks old was, on average, softer than SHR's at the same age ($p = 0.059$). Interestingly, similar results were observed for the common carotid artery by Lichtenstein *et al.* [27] who compared, under static transmural pressures, SHR with normotensive Wistar-Kioto (WKY) rats. On the other hand, strain (ε_{yy}) is a relative measure that primarily depends on the pressure gradient ($\Delta P \equiv$ systolic pressure - diastolic pressure, in this case) and on the tissue stiffness. To provide an absolute and more robust characterization parameter of the vessel wall, ε_{yy} can be normalized with ΔP to estimate the elastic modulus. In the case where the pressure monitoring system would not allow appropriately measuring ΔP, another option could be to normalize the strain with respect to the heart rate and the imaging system frame rate, since they both may have influence on the elastographic measurement process. These options will both be of interest in further investigations.

Unfortunately, the relatively low frame rate of the RF data acquisition system (Vevo 660) constituted a drawback of the current study. Indeed, the higher the frame rate, the more correlated are the RF images within a sequence, improving the strain estimation. Additionally, the higher the frame rate, the shorter is the time elapsed between successive RF images within the time-sequence data set, and thus the lower will be the strain estimates. This also explains high strain values (up to 6.76%) computed for the carotid arteries with MicroNIVE in this study. It is important to note that the new Vevo 770 ultrasound system, commercialized by Visualsonics, now provides up to 120 images/s (full field of view) to 240 images/s (zoomed view).

5.3. About MicroNIKE data

In vitro preliminary data on a fresh excised kidney clearly allowed identifying the medulla with specific quantitative mechanical properties. An ascending slope profile was observed in Fig. 3c for the longitudinal elastogram. This artifact results from the application of a non uniform external stress to compress the kidney. On the other hand, the transversal elastogram allowed artifact-free images and the identification of the medulla with around 0.25 % strain. Whereas we are aware that the application of external compression could be tedious in vivo, namely due to the presence of fatty tissue located between the skin and the kidney, these results give confidence in the potential of MicroNIKE to phenotype rat models of hypertension using kidney's mechanical properties. Furthermore, in future experiments, it would be of interest to monitor the external applied stress to enable elastic modulus assessments that are known to be more appropriate than strains to characterize biological soft tissues.

6. CONCLUSION

This paper has addressed the feasibility of using the vessel wall (MicroNIVE) and the kidney (MicroNIKE) mechanical properties as potential phenotypes of hypertension in rat models. In the case of MicroNIVE, *in vivo* data were reported on SHR and BN rats showing SHRs' carotid arteries stiffer than that of BN at 15-weeks old. Regarding MicroNIKE, *ex vivo* data on an RI's excised kidney clearly demonstrated the potential of the method to identify and characterize different structures within this organ. In summary, combining novel *in vivo* imaging technologies with state of the art transgenic rodent models may represent unprecedented tools for gene identification in hypertension, which is part of our future investigations. The availability of MicroNIVE and MicroNIKE could lead to significant new discoveries in the fields of the pathophysiology and pharmacogenetics of hypertension.

7. ACKNOWLEDGEMENTS

REFERENCES

[1] Joffres MR, Hamet P, Maclean DR, L'Italien GJ, Fodor G. Distribution of blood pressure and hypertension in Canada and the United States. *Am J Hypertension*. 2001;14:1099-1105.

[2] Ezzati M, Lopez AD, Rodgers A, Vander HS, Murray CJ. Selected major risk factors and global and regional burden of disease. *Lancet*. 2002;360(9343):1347-1360.

[3] Dutil J, Eliopoulos V, Tremblay J, Hamet P, Charron S, and Deng AY. Multiple quantitative trait loci for blood pressure interacting epistatically and additively on Dahl rat chromosome 2. *Hypertension*. 2005;45:557-564.

[4] Mulvany MJ. Modeling the vasculature: A judicious approach? Hypertension. 2005;46(4):652-653.

[5] Intengan HD, Schiffrin EL. Mechanical properties of mesenteric resistance arteries from Dahl salt-sensitive rats: Role of endothelin-1. *Journal of Hypertension*. 1998;16:1907-1912.

[6] LLoyd-Jones DM, Bloch KD. The vascular biology of nitric oxide and its role in atherogenesis. Ann Rev Med. 1996;47:365-375.

[7] Marin, R., Gorostidi, M., Fernandez-Vega, F., and Alvarez-Navascues, R., "Systemic and glomerular hypertension and progression of chronic renal disease: the dilemma of nephrosclerosis," Kidney Int.Suppl, no. 99, pp. S52-S56, Dec.2005.

[8] Zhao J, Day J, Yuan ZF, and Gregersen H. Regional artery stress-strain distributions referenced to the zero-stress state in the rat. *Am J Physiol Heart Circ Physiol*. 2002;282:H622-H629.

[9] Pravenec M and Kren V. Genetic analysis of complex cardiovascular traits in the spontaneously hypertensive rat. *Exp Physiol*. 2005;90(3):273-276.

[10] Dumas P, Sun Y, Corbeil G, Tremblay S, Pausova Z, Kren V, Krenova D, Pravenec M, Hamet P, and Tremblay J. Mapping of quantitative trait loci (QTL) of differential stress gene expression in rat recombinant inbred strains. *J Hypertension*. 2000;18(5):545-551.

[11] Hubner N, Wallace CA, Zimdahl H, Petretto E, Schulz H, Maciver F, Mueller M, Hummel O, Monti J, Zidek V, Musilova A, Kren V, Causton H, Game L, Born G, Schmidt S, Muller A, Cook SA, Kurtz TW, Whittaker J, Pravenec M, and Aitman TJ. Integrated transcriptional profiling and linkage analysis for identification of genes underlying disease. *Nat Genet*. 2005;37(3):243-253.

[12] Safar M. Arteries in Clinical Hypertension. *Lippincott – Raven Publishers*. 1996.

[13] Ophir J, Céspedes E I, Ponnekanti H, Yazdi Y, and Li X. Elastography: A quantitative method for imaging the elasticity in biological tissues. *Ultrasonic Imaging*. 1991;13(2):111-134.

[14] Garra BS, Céspedes EI, Ophir J, Spratt SR, Zuurbier RA, Magnant CM, and Pennanen MF. Elastography of breast lesions: Initial clinical results. *Radiology*. 1997;202(1):79-86.

[15] Lorenz A, Sommerfeld HJ, Garcia-Schurmann MG, Philippou S, Senge T, and Ermert H. A new system for the acquisition of ultrasonic multi-compression strain images of human prostate in vivo. *IEEE-Ultrasonics Ferroelectrics Frequency Control*. 1999;46(5):1147-1154.

[16] Pesavento A, Lorenz A, Siebers S, and Ermert H. New real-time strain imaging concepts using diagnostic ultrasound. *Phys Med Biol*. 2000;45:1423-1435.

[17] de Korte CL, Pasterkamp G, Van der Steen AFW, Woutman HA, and Bom N. Characterization of plaque components with intravascular ultrasound elastography in human femoral and coronary arteries in vitro. *Circulation*. 2000;102(6):617-623.

[18] de Korte CL, Van der Steen AFW, Céspedes EI, Pasterkamp G, Carlier SG, Mastik F, Schoneveld AH, Serruys PW, and Bom N. Characterization of plaque components and vulnerability with intravascular ultrasound elastography. *Physics in Medicine & Biology*. 2000;45(6):1465-1475.

[19] Maurice RL, Ohayon J, Finet G and Cloutier G. Adapting the Lagrangian Speckle Model Estimator for Endovascular Elastography: Theory and Validation with Simulated Radio-Frequency data. *JASA*. 2004;116(2): 1276-1286.

[20] Maurice RL, Brusseau É, Finet G, Cloutier G. On the potential of the Lagrangian speckle model estimator to characterize atherosclerotic plaques in endovascular elastography: In vitro experiments using an excised human carotid artery. *Ultrasound Med & Biology*. 2005;31:85-91.

[21] Maurice RL, Fromageau J, Brusseau É, Finet G and Cloutier G. On the Potential of the Lagrangian Speckle Model Estimator for Endovascular Elastography : In vivo Human Coronary Study. *Ultrasound in Medicine & Biology*. 2007 (in press).

[22] Bang J, Dahl T, Bruinsma A, Kaspersen JH, Hernes TAN, and Myhre HO. A new method for analysis of motion of carotid plaques from RF ultrasound images. *Ultrasound in Med & Biol*. 2003;29(7):967-976.

[23] Mai JJ, Insana M. Strain imaging of internal deformation. *Ultrasound in Med & Biol*. 2002;28(11/12):1475-1484.

[24] Maurice RL, Ohayon J, Frétigny Y, Bertrand M, Soulez G, and Cloutier G. Non-invasive vascular elastography: Theoretical framework. *IEEE Trans on Med Imaging*. 2004;23(2):164-180.

[25] Maurice RL, Daronat M, Ohayon J, Stoyanova É, Foster SF, and Cloutier G. Non-invasive high-frequency vascular ultrasound elastography. Physics in Medicine & Biology. 2005;50:1611-1628.

[26] Maurice RL and Bertrand M. Lagrangian speckle model and tissue-motion estimation – Theory. IEEE Trans on Med Imaging. 1999;18(7):593-603.

[27] Lichtenstein O, Safar ME, Mathieu E, Poitevin P, and Levy BL. Static and dynamic mechanical properties of the carotid artery from normotensive and hypertensive rats. *Hypertension*. 1998;32:346-350.